


Article

Mapping Crop Leaf Area Index and Canopy Chlorophyll Content Using UAV Multispectral Imagery: Impacts of Illuminations and Distribution of Input Variables

Wenjuan Li ^{1,*}, Marie Weiss ² , Bernard Garric ³, Luc Champolivier ³, Jingyi Jiang ⁴, Wenbin Wu ¹ and Frédéric Baret ²

¹ State Key Laboratory of Efficient Utilization of Arid and Semi-Arid Arable Land in Northern China, The Institute of Agricultural Resources and Regional Planning, Chinese Academy of Agricultural Sciences, Beijing 100081, China

² INRAE, Avignon Université, UMR EMMAH, UMT CAPTE, 84000 Avignon, France

³ Terres Inovia, 6 Chemin de la Côte Vieille, 31450 Baziege, France

⁴ The College of Forestry, Beijing Forestry University, Beijing 100083, China

* Correspondence: liwenjuan01@caas.cn

Abstract: Leaf area index (LAI) and canopy chlorophyll content (CCC) are important indicators that describe the growth status and nitrogen deficiencies of crops. Several studies have been performed to estimate LAI and CCC using multispectral cameras onboard an unmanned airborne vehicle (UAV) system. However, the impacts of illuminations during UAV flight and problems of how to invert still need more investigation. UAV flights with a multispectral camera were performed under clear (diffuse ratio 0) and cloudy illumination conditions (diffuse ratio 1) over rapeseed, wheat and sunflower (only clear) fields. One-dimension radiative transfer model PROSAIL was run twice to generate a clear-sky model and a cloudy-sky model, respectively. The LAI and CCC of flights under a clear sky were inverted from the clear-sky model, and the flights under cloudy conditions were inverted from both clear-sky and cloudy-sky models to compare the results. Moreover, three Look-Up-Tables (LUT) were built with same input variables but different distributions of LAI. Results showed that LAI from uniform dense LUT had better correspondence with ground measurements for all crops ($R^2 = 0.51\sim 0.69$). The illumination condition had little impact on small to medium LAI ($LAI < 5$) and CCC. However, the inversion of imageries during cloudy sky conditions from the clear-sky model led to an overestimation of high LAI values.

Keywords: leaf area index (LAI); canopy chlorophyll content (CCC); UAV; multispectral camera; look-up-table



Citation: Li, W.; Weiss, M.; Garric, B.; Champolivier, L.; Jiang, J.; Wu, W.; Baret, F. Mapping Crop Leaf Area Index and Canopy Chlorophyll Content Using UAV Multispectral Imagery: Impacts of Illuminations and Distribution of Input Variables. *Remote Sens.* **2023**, *15*, 1539. <https://doi.org/10.3390/rs15061539>

Academic Editor: Fernando Pérez-Cabello

Received: 15 February 2023

Revised: 5 March 2023

Accepted: 9 March 2023

Published: 11 March 2023



Copyright: © 2023 by the authors. Licensee MDPI, Basel, Switzerland. This article is an open access article distributed under the terms and conditions of the Creative Commons Attribution (CC BY) license (<https://creativecommons.org/licenses/by/4.0/>).

1. Introduction

The accurate mapping of spatial variability of a field during the growing season is an important step for precision agriculture practice [1,2]. Mapping key parameters that are closely related to canopy status can provide useful diagnostic information about the field, which assists in crop management, yield forecasting and environmental protection for farmers [3].

Remote sensing-based mapping methods have been deployed by several studies on a variety of platforms in precision farming, with satellites and full-size aircraft [4,5]. On board optical sensors such as multispectral, hyperspectral or thermal infrared cameras acquire bulk images of the ground. However, the satellite-based imageries are limited by coarse spatial resolution that cannot satisfy some applications that need high spatial resolution (such as weed detection and management), or over small fields [6], or in cloudy weather conditions occurring at key growing dates [7,8]. Further, full-size aircraft is expensive and the flying altitude is restricted by local policies, buildings and the natural environment.

Therefore, there is a need to develop techniques for the rapid acquisition of high spatial and temporal resolution data during critical crop development periods at economic costs. A low-altitude remote sensing system by the UAV provides a practical substitute for the platforms mentioned above [9]. These UAVs are always lightweight with a minimal cost of flight time. Equipped with a new developed small RGB, multispectral, hyperspectral or thermal infrared sensors, the UAV systems can monitor the crop conditions at large areas in a high spatial (centimeter) and at key stages of plant development [3,10].

Recently, several crop key traits have been measured using sensors mounted on UAV systems [11–14]. Among these traits, leaf area index (LAI) and chlorophyll content are two biophysical variables that are frequently used in the precision agriculture domain. LAI is defined as half the total green area of leaves per unit of horizontal ground area [15]. It reflects the potential growth of the canopy and is a key variable for biomass and yield estimation. Chlorophyll content is an important indicator of photosynthesis activity, which is related to the nitrogen concentration in green vegetation and serves as a measure of the crop response to nitrogen application [16]. This quantity can be calculated both at the leaf level (leaf chlorophyll content, Cab) and at the canopy level (Canopy Chlorophyll content, CCC) by multiplication of the leaf level chlorophyll content and LAI. Studies have demonstrated that a direct estimation of CCC is more robust and accurate on the estimation of canopy nitrogen content, vegetation physiological status and plant stress [5,17–19]. Mapping spatial variability of LAI and CCC has, therefore, been preferred for its implications for the variation of biomass and nitrogen concentration in the field.

Previous studies on LAI and CCC estimations from satellites have mostly been conducted under clear illumination conditions without the contamination of clouds. However, in the measurements by UAV, cloud influence is an inevitable factor that cannot be ignored, especially in regions with frequent cloud visits during the key growing stages [20–22]. Few experiments have been conducted to explore the inversion of LAI and CCC under cloudy conditions.

Among the different methods used to retrieve LAI and CCC from reflectance, Look-Up-Tables are quite popular since they are fast, accurate and can avoid the local minimum that may happen on iterative convergence algorithms [23,24]. A key point that influences the accuracy of retrieval performances is the distribution of the radiative transfer model input parameters used to build the LUT [25,26]. The distribution of LAI is the most important among other parameters. Ref. [12] uses uniform distribution for LAI and Gaussian distribution for other parameters, while [27] used uniform distribution for all parameters. Ref. [4] used the truncated Gaussian distribution for all parameters including LAI, although using a neural network inversion algorithm. The uniform distribution can obtain more even performances, while the Gaussian distribution set prior information on the crops, which is good for specific crops but may not be applicable for several crop variables in structures. Nevertheless, the uniform distribution is greatly influenced by sparse steps. Therefore, a new distribution is necessary.

This study was conducted in the context of the French project PRECIDRONE that aims to provide operational decision-making tools to farmers and help them spatially optimize nitrogen fertilization and their water supply practices in the context of sustainable agriculture. Maps of LAI and CCC were therefore important to be used as inputs of crop models to estimate the crop nitrogen concentration and biomass. The objective of this paper is, thus, to implement a generic algorithm to estimate LAI and CCC at field level based on LUT, to evaluate it over different crops, and to study the influences of illumination and distributions of input variables. We first present the study sites, the associated ground data and the multispectral camera and UAV system. Then, the processing of the images is described, including the generation of the orthoimages from the data acquired by the camera, and the LAI and CCC estimation algorithm based on LUTs. The impacts of illuminations and input variables distributions are analyzed and the relationship between LAI and biomass, canopy nitrogen content and CCC were investigated.

2. Materials and Methods

2.1. Experiment Sites and Ground Measurements

The experimental sites are distributed close to Toulouse, in the south-west of France. This region experiences a typical temperate continental climate, with hot and dry summer and cold and humid winter. Three crops were involved in this field campaign: rapeseed, sunflower and wheat. Rapeseed is sown from mid-August to mid-September, wheat is sown from October to November and harvested at the beginning of July, while sunflower is a summer crop planted from mid-April to mid-May and harvested around September. For each crop type, several fields were selected. They were under contrasted growth conditions due to fertilization, soil type, topography or cultivar, yet dominant with lowest weed coverage. The homogeneity of wheat and rapeseed fields was good, while the sunflower fields' plant densities were quite heterogeneous. On each field, one or several 1 m² microplots were selected for ground measurements. The positions of these 61 microplots were recorded by a GPS. The microplots were marked using bright ground control points easily detectable on the UAV imagery. The dates for all ground measurements were close to the UAV flights (Table 1).

Table 1. The names, coordinates, dates and weather of the UAV flights for rapeseed, sunflower and wheat fields.

Crop	Field Name	Center Coordinate (N, E, °)	Flight Date	Weather	
Rapeseed	AURIAC	43.52, 1.82	20/01/2016	Cloudy	
	BAZIEGE	43.47, 1.63	13/01/2016	Clear	
	CARAMAN 1		43.54, 1.77	04/12/2015	Cloudy
			14/01/2016	Cloudy	
	CARAMAN 2		43.55, 1.76	04/12/2015	Cloudy
			14/01/2016	Cloudy	
	DELM 1		43.529, 1.66	02/12/2016	Cloudy
			13/01/2016	Clear	
	DELM 2		43.528, 1.660	02/12/2015	Cloudy
			13/01/2016	Clear	
	DELM 3		43.527, 1.661	02/12/2015	Cloudy
			13/01/2016	Clear	
	GRANGETTES 1		43.478, 1.707	03/12/2015	Clear
			20/01/2016	Cloudy	
GRANGETTES 2		43.479, 1.708	03/12/2015	Clear	
		20/01/2016	Cloudy		
Sunflower	FRANDAT-01	43.99, 0.66	06/07/2016	Clear	
	FRANDAT-13	43.97, 0.65	06/07/2016	Clear	
	FRANDAT-27	43.98, 0.72	06/07/2016	Clear	
	FRANDAT-29	43.98, 0.71	06/07/2016	Clear	
Wheat	ST-JEAN-POUTGE-1		05/02/2016	Clear	
			30/03/2016	Clear	
	VIC-FEZENSAC-1	43.73, 0.31	10/02/2016	Cloudy	
			30/03/2016	Clear	
	VIC-FEZENSAC-2	43.73, 0.29	10/02/2016	Cloudy	

Table 1. *Cont.*

Crop	Field Name	Center Coordinate (N, E, °)	Flight Date	Weather
	VIC- FEZENSAC-4	43.74, 0.30	10/02/2016	Cloudy
	VIC- FEZENSAC-3	43.74, 0.28	10/02/2016	Cloudy
			30/03/2016	Clear

Nitrogen content and fresh biomass were measured by cutting all the leaves within each 1 m² microplot. The sampled leaves were first weighed to obtain the green fresh biomass, and then heated in an oven at 80° for 36 h for weighing the dry biomass. Finally, the dried leaves were used for the determination of nitrogen content. The nitrogen contents were measured for rapeseed and sunflower microplots.

The LAI measurements were taken over a homogeneous region close to the microplot of each field. On rapeseed and wheat fields, LAI was measured using the Sony ILCE α5100L RGB camera with 6024 × 4024 pixels inclined at 57° and 1.5 m far away from the ground. Ten to fifteen photos were taken close to the microplot along the sowing direction, facing the sun to limit shadow influences. On sunflower fields, around 10 photos were taken using a digital camera equipped with a hemispherical lens at nadir direction. All the images were then processed using the CAN-EYE software (<https://www6.paca.inra.fr/can-eye>, V6.3, accessed on 14 May 2016) to retrieve LAI.

The leaf chlorophyll content was measured using the SPAD device [28] with a minimum of 15 leaves randomly located at the top of the canopy. These SPAD raw readings were converted into arial content of chlorophyll (µg/cm²) using the equation by [29] and then averaged over each field.

2.2. UAV and Camera System

An unmanned aircraft drone DT18 AG was used in this campaign. It can fly for 2 h at a speed of 60 km/h and a height ranging from 70 m to 150 m. Onboard the drone, a MicaSense RedEdgeTM multispectral camera was mounted. It can simultaneously acquire images in five discrete spectral bands: blue (475 nm), green (560 nm), red (668 nm), red-edge (717 nm) and near infra-red (840 nm). The spectral resolution at a Full Width at Half Maximum (FWHM) was 20 nm for blue and green bands, 10 nm for red and red-edge bands and 40 nm for NIR band. The image resolution was 1280 × 960 pixels, and optical focal length was 5.5 mm, yielding a horizontal field of view of the camera around 47.2°. Images were taken per second and stored in a 12-bit TIFF format.

On each field, the flight was achieved in around 10–20 min. The nominal ground sample distance of these images was around 8 cm per pixel, with the flight altitude at 120 m. The sky was clear and wind speed was low for a major part of the flights, but was cloudy or partly cloudy for the other flights (Table 1).

2.3. Orthoimage of Multispectral Reflectance

The Pix4D software (<https://pix4d.com/>, accessed on 14 May 2016) was used to generate the ortho-projected multispectral reflectance image automatically from all the images acquired during each flight. This process included the alignment of images according to the GPS information, the reconstruction of the 3D surface model, the calibration of reflectance of images and the generation of orthomosaic images. The reflectance images were then calibrated using images acquired over a calibration body (isotopic white panel name) prior to each flight [30] to obtain the reflectance images. The generated ortho-image had a spatial resolution around 8 cm. It was then aggregated into 1 m by a simple averaging method in order to satisfy the turbid medium assumption over each pixel required by the use of a one-dimension canopy radiative transfer model to retrieve LAI from the reflectance [31].

2.4. Estimation of LAI and Canopy Chlorophyll Content

A look up table (LUT)-based inversion method was used to generate an image of LAI and chlorophyll from the reflectance orthoimage. The LUT was built according to a one-dimension radiative transfer model PROSAIL [32], which is a combination of canopy radiative transfer model SAIL [31] and a leaf optical properties model PROSPECT [33].

At the canopy level, the LUT was generated by running the PROSAIL model in the forward mode with input variables listed in Table 2. Three different LUTs were generated, with the same input variables but different distributions.

- Gaussian LUT (LUT-G)

Table 2. Distribution of PROSAIL input variables to generate the Gaussian distribution LUT. *ALA* = Average Leaf Angle inclination; *HsD* = Hot-spot parameter; *N* = leaf structure parameter; *C_{ab}* = chlorophyll content; *C_{dm}* = dry matter content; *C_w* = leaf water content; *C_{bp}* = brown pigment concentration; *B_s* = soil brightness; *skyl* = diffuse ratio. More information about the variables' values can be found in [4].

Variable	Minimum	Maximum	Mean	Standard Deviation	Distribution
<i>LAI</i>	0	10	2	2	Gauss
<i>ALA</i> (°)	30	80	60	20	Gauss
<i>HsD</i>	0.1	0.5	0.2	0.5	Gauss
<i>N</i>	1.2	2.2	1.5	0.3	Gauss
<i>C_{ab}</i> ($\mu\text{g}\cdot\text{cm}^{-2}$)	20	90	45	30	Gauss
<i>C_{dm}</i> ($\text{g}\cdot\text{cm}^{-2}$)	0.003	0.011	0.005	0.005	Gauss
<i>C_w</i>	0.6	0.75	0.75	0.08	Gauss
<i>C_{bp}</i>	0	0.08	0	0.3	Gauss
<i>B_s</i>	0.5	2	-	-	Gauss
<i>skyl</i>	0	0	-	-	-

The LUT-G was defined that all input variables follow a Gaussian distribution, with the range and distribution law shown in Table 2. The Gaussian distribution law is consistent with the one used in [4]. In total, 55,296 combinations of input variables were generated. Specifically, the distribution of LAI and $\text{LAI} \times C_{ab}$ is shown in Figure 1.

- Uniform LUT (LUT-U)

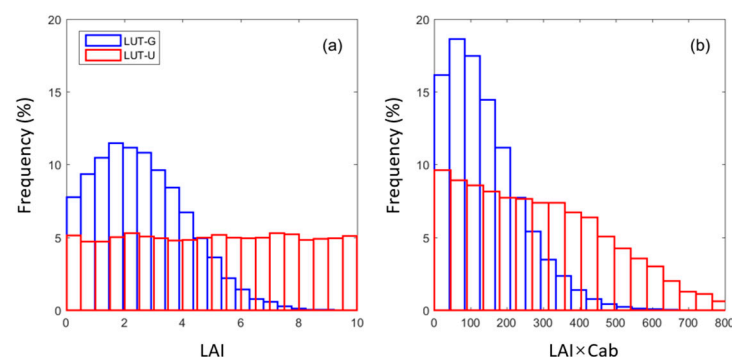


Figure 1. Distribution law of (a) LAI and (b) $\text{LAI} \times C_{ab}$ for Gaussian LUT and uniform LUT.

The LUT-U was generated by setting the distribution of LAI to uniform within the minimum and maximum range shown in Table 2. The other variables follow same distribution as Gaussian LUT. The final size of the LUT-U was 13,824. The distribution of LAI and $\text{LAI} \times C_{ab}$ is shown in Figure 1.

- Uniform dense LUT (LUT-UD)

One limitation of LUT is that the density of input variables greatly influences the inversion. Therefore, a dense LUT was proposed to check if the estimation would be more accurate. Based on uniform LUT, LAI was separated into 10 categories with a step of 1, such as 0–1, 1–2, . . . 9–10. For each category of LAI, an LUT was generated with LAI in the uniform distribution and the other variables following same distributions as Gaussian LUT (Table 2). Finally, 10 LUTs in the size of 13,824 cases were generated.

For the 3 LUTs, a full orthogonal experimental plan was adopted to combine the 9 input variables by splitting the whole range of variation of each variable into a small number of classes. This allowed populating more evenly the 9 dimensions of the space of canopy realization.

For wheat fields, 5–10 soil samples were collected in the field and the reflectance was measured in the lab. For the other fields, as no spectrum acquisition was performed, we manually selected several soil pixels from the orthoimage at 8 cm resolution by assuming that the reflectance in the blue, green, red and NIR bands continuously increased and the NDVI was smaller than 0.2. These ground measured or image selected soil reflectance profiles were compared with a soil database, which includes the reflectance of a large range of soil types [34]. The five closest soil profiles were extracted from the database. A soil brightness factor was then multiplied to the five selected soil profiles to simulate further variations of soil reflectance due to roughness, directional effects of observations and moisture. The same soil reflectance will be used for all three LUTs.

For all three LUTs, the PROSAIL model was run in a forward direction two times using different diffuse ratio values ($skyl = 0$ or 1). The model with $skyl = 0$ is called ‘clear-sky model’ in the following context, and the other with $skyl = 1$ is called ‘cloud-sky model’. Note that there is no ground measurement of diffuse ratio since it is not easy in an operational way.

To decrease the size and dimension of the LUT, the viewing angle was set to nadir only since we only consider orthoimages. For each combination of variables, the canopy reflectance was simulated and aggregated to each band according to the spectral response function of the multispectral camera.

For each pixel of the resampled orthoimage (1 m spatial resolution), a cost function was generated to calculate the RMSE between measured surface reflectance and simulated reflectance in the LUT (Equation (1)). The relative reflectance with the NIR band was used in order to minimize the illumination variation between calibration and flight acquisitions (Verger et al., 2014).

$$J = \frac{\sum_{i=1}^4 \left(\frac{BRF_i}{BRF_{NIR}} - \frac{\widehat{BRF}_i}{\widehat{BRF}_{NIR}} \right)^2}{4} \quad (1)$$

where BRF_i and \widehat{BRF}_i are measured and simulated reflectance on band i .

J was sorted and the first 50 smallest cases were found. For LUT-G and LUT-U, the median values of corresponding LAI and chlorophyll were calculated and used as the inverted results for the pixel. For LUT-UD, the LAI value was firstly estimated from LUT-U, e.g., LAI0. Then, a dense LUT in the range of $[LAI0 + 0.5, LAI0 - 0.5]$ was searched. The measured reflectance of the pixel was compared with the ones in the specific dense LUT using the cost function (Equation (1)), as shown above. The median values of LAI and Cab of the first 50 smallest cases from the dense LUT were used as the results for the pixel. CCC was computed as $LAI \times C_{ab}$.

3. Results

3.1. Impacts of the Distribution of Input Variables for LUT Generation

LAI retrieved from Gaussian LUT, uniform LUT and uniform dense LUT were compared with ground measurements for rapeseed, wheat and sunflower. For all three LUTs, the points under cloudy conditions were inverted by the LUT generated from the diffuse model, and the points under clear conditions were inverted by the LUT from the direct model.

Results showed that the LAI from three LUTs correlated better with ground measurements for rapeseed and wheat than sunflower (Figure 2, Table 3). This is mainly because of the heterogeneity of sunflower fields, which influences the representativeness of ground measurements compared with UAV flights. For rapeseed, the Gaussian LUT and uniform LUT have similar performances, while the uniform dense LUT shows a better RMSE of 0.36 and a higher correlation of 0.69. For sunflower, the uniform dense LUT greatly improves the inversion accuracy compared to Gaussian LUT by RMSE of 0.07. For wheat, the estimated LAI from dense LUT showed the best correspondence ($R^2 = 0.62$) but highest variation (RMSE = 1.23) compared with those from Gaussian distribution. Gaussian LUT had small distributions at LAI larger than five; therefore, there are no high estimations compared to the other LUTs.

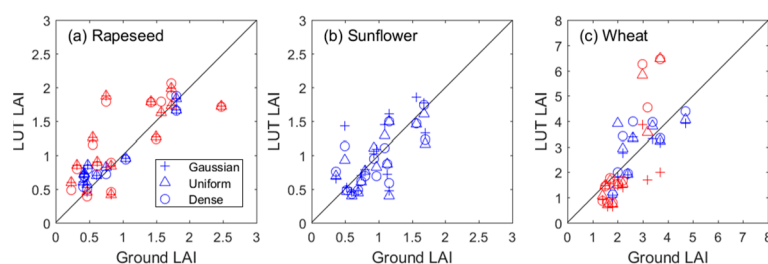


Figure 2. Comparison of inverted LAI from three LUTs (Gaussian, Uniform and Uniform Dense) with the ground measurements. Symbols in red correspond to UAV flights under clouds conditions, and symbols in blue correspond to those under clear illuminations.

Table 3. Statistics of inverted LAI from three LUTs (Gaussian, Uniform and Uniform Dense) with ground measurements (R^2 and RMSE in bracket).

	Rapeseed	Sunflower	Wheat
Gaussian	0.65 (0.39)	0.42 (0.37)	0.58 (0.83)
Uniform	0.65 (0.39)	0.49 (0.31)	0.55 (1.17)
Uniform Dense	0.69 (0.36)	0.51 (0.30)	0.62 (1.23)

3.2. Impacts of Illumination Conditions

The impacts of illumination conditions were firstly studied using the modelling method. Reflectance under clear-sky conditions ($skyl = 0$) and under cloudy-sky conditions ($skyl = 1$) were simulated using the PROSAIL model, with same input variables shown in Table 2. LAI and C_{ab} for reflectance under each illumination condition were inverted using the uniform dense LUT (simulated under clear sky condition). Then, the inverted LAI and C_{ab} were compared with the original input ones. Figure 3 shows that LAI from both input reflectance were similar at small values, but LAI from reflectance under the cloudy-sky condition shows higher values and more saturations. On the other hand, C_{ab} from two reflectance is similar, although the one from the cloudy-sky condition showed slightly scatterings.

The influence of the illumination condition was also assessed using actual ground measurements over UAV flight acquired on Vic-4 wheat field under cloudy conditions. The uniform dense LUT was used in the inversion. The results showed that the estimated LAI from the clear-sky model were consistent with those from the cloudy model at small and medium LAI values ($LAI < 5$), but they were larger than the latter at high LAI values (Figure 4a–c). For C_{ab} , the differences between using the clear-sky model or cloudy model are not obvious, except for some pixels at high values ($C_{ab} > 65 \mu\text{g}\cdot\text{cm}^{-2}$). Under cloudy conditions, the leaves tend to show lower reflectance at NIR band and higher reflectance at red band than under clear-sky condition. Therefore, the inversion using the clear-sky model should obtain higher LAI values to satisfy the lower NIR reflectance.

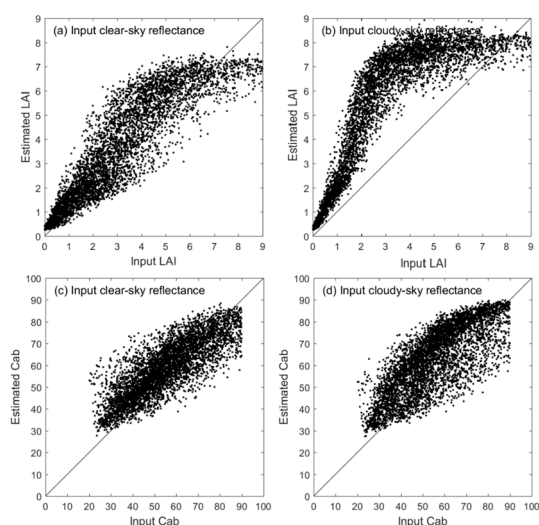


Figure 3. The regression of input LAI and estimated LAI from simulated clear-sky reflectance (a) and cloud-sky reflectance (b). (c,d) are corresponding for C_{ab} ($\mu\text{g}\cdot\text{cm}^{-2}$).

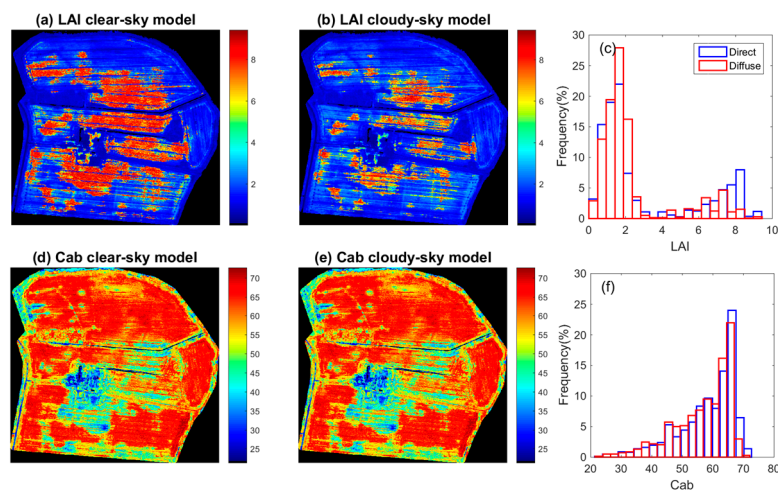


Figure 4. Spatial distribution of LAI and C_{ab} from clear-sky model and cloudy model and the distribution of corresponding values over Vic-4 wheat field in 2016. (c,f) represent the distribution of LAI and C_{ab} , respectively. ‘Direct’ and ‘Diffuse’ on (c,f) correspond to ‘clear-sky’ and ‘cloud-sky’ models, respectively. (a) LAI clear-sky model. (b) LAI cloudy-sky model. (d) Cab clear-sky model. (e) Cab cloudy-sky model.

The comparison with ground measurements further demonstrates the influence of using a clear-sky model on the measurement under cloudy conditions. Figure 5 shows that the validation accuracy is improved greatly for wheat after using the cloudy model on measurements under cloudy conditions when LAI is larger than 5 (Figure 5a,b, RMSE decreases from 1.98 to 1.23). However, changing the model on cloudy pixels has small influences on small LAIs of rapeseed (LAI < 5, Figure 5d). This is consistent with the results observed by [12]; that the illumination has minor effects on the inversion of small LAI when the normalization in the cost function is used. The cloudy pixels still show overestimation to some extent at high LAI values (LAI > 5), even if the diffuse model is used. This might also be because of the saturation of reflectance at high values. The higher LAI values are generally much more difficult to estimate due to the reduction in sensitivity of reflectance to LAI.

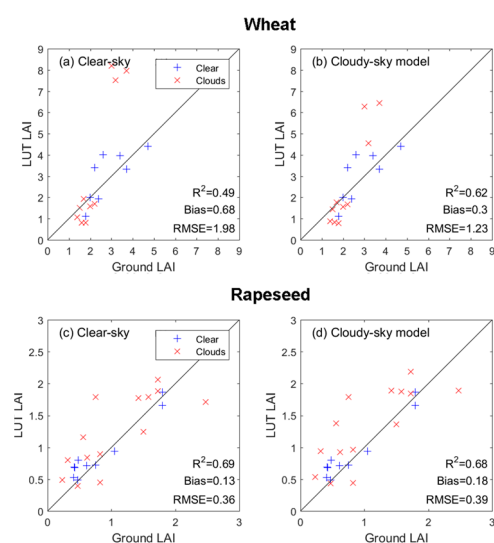


Figure 5. The comparison between inverted LAI and ground measured LAI for wheat and rapeseed. (a,c) All the points are inverted from direct model only, (b,d) points under clear conditions were inverted by direct model, and points under cloudy conditions were inverted by diffuse model.

3.3. Comparison with Ground Canopy Nitrogen Content

The relationship between UAV estimated canopy chlorophyll content and ground measured canopy nitrogen content was studied in Figure 6. For rapeseed, the estimated canopy chlorophyll is very well correlated with ground nitrogen content, indicating that the estimated value from UAV flights can be used to predict the ground nitrogen when the ground data are not available. For sunflower, the relationship between canopy chlorophyll and ground nitrogen shows some scattering, although a good correlation is observed ($R^2 = 0.52$). This might be because of the heterogeneity of the sunflower fields, which leads to big variations between the microplots for nitrogen measurements and the one for LAI measurements.

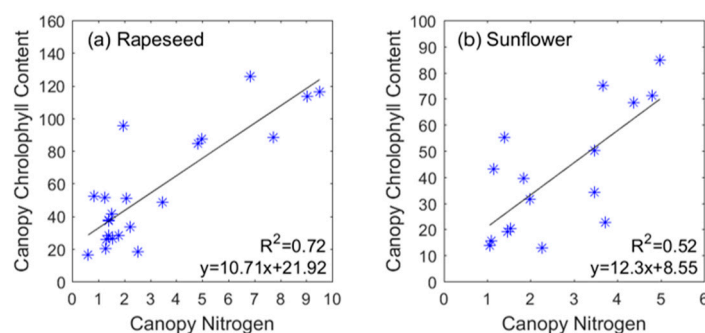


Figure 6. Comparison of estimated canopy chlorophyll content ($LAI \times C_{ab}$, $\mu\text{g}/\text{cm}^2$) with ground measured canopy nitrogen content (g/m^2) for rapeseed and sunflower. LAI and C_{ab} are estimated from uniform dense LUT. * represents the scatter points.

3.4. Comparison with Ground Biomass

Figure 7 illustrates that the LAI estimated from UAV flights has a very good correlation with the ground measured fresh biomass quantity for rapeseed and wheat, indicating that the LAI can be used to describe the variation of fresh biomass in the field. For sunflower, the correlation is low, mainly because of the extreme high biomass values for low LAI canopy ($LAI < 1$, biomass $> 1500 \text{ g}/\text{m}^2$) from two measurements. The heterogeneity of sunflower fields produces the large discrepancy. After removing the two points, the R^2 increases from 0.2 to 0.52, indicating the potential to estimate biomass from LAI for sunflower.

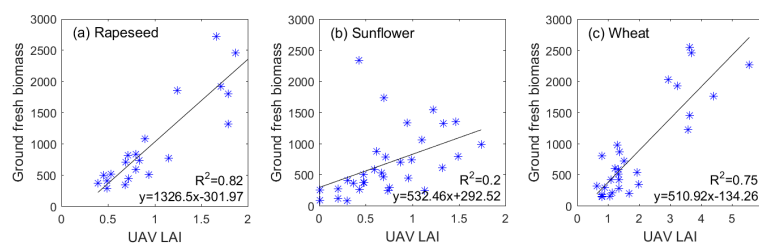


Figure 7. Regression between UAV estimated LAI from the uniform dense LUT and ground measured biomass quantity (g/m²). * represents the scatter points.

4. Discussion

We proposed a generic inversion algorithm to estimate LAI and CCC over crop fields using UAV multispectral imageries. Since the distribution of LAI has large impacts on the inversion, we compared LUT with different LAI distribution and studied the impacts on inversion results. Compared with Gaussian LUT and uniform LUT in the size of 13,824, the dense uniform LUT has a much larger size (10 × 13,824). This is beneficial to biophysical inversion because the accuracy of model retrieval depends on the size of LUT [35], e.g., [36] generated an LUT of 100,000 sets to obtain a good estimation of LAI. Moreover, we proposed a new method to generate a dense LUT by setting LAI into several categories and adding more LAI in each category. This could improve the representativeness of LAI evenly and contribute to better inversion results. Nevertheless, the distribution of chlorophyll content and other input variables might also have impacts on the final inversion results. Additionally, the impacts of distribution of these variables on different inversion algorithms, e.g., neural network and LUT, also need more investigations.

Unlike optical satellite observations that are only available under ideal clear sky conditions, the illumination conditions during UAV flights for breeding and precision agriculture purposes can vary, e.g., clear-sky, overcast or with moving clouds [21,22]. It is not practical to only collect data under one specific illumination condition in real natural environments. Building a generic algorithm to estimate accurate and stable LAI and CCC under various illumination conditions is, therefore, important. To our knowledge, the effects of clouds on UAV multispectral imagery have attracted attention in the last few years. However, most of the studies were focused on spectral reflectance or vegetation indices [20,22]. Notably, fewer studies were conducted on the impacts of illumination variation on biophysical variables inversion. We conducted preliminary investigations on this aspect. However, only ideal clear conditions and totally cloudy sky were considered in this study. In the future, more investigations on impacts of illumination under various cloud cover conditions will be conducted and an applicable solution for the LAI and *Cab* retrieval will be proposed. Moreover, the diffuse ratio of radiation on each wavelength should be measured at the ground level and used as input for the model inversion, in order to improve the inversion accuracy. The accuracy of incorporating a diffuse ratio to the modelling and inversion processes should be studied further.

The results in this study indicate that canopy nitrogen content can be predicted well from canopy chlorophyll content, which is consistent with findings from previous studies [5,37]. However, more research is still needed to investigate whether the correlation can be improved for heterogeneous fields and crops with complex structures, e.g., sunflower. Furthermore, phenological stages also have impacts on the relationship between canopy chlorophyll content and canopy nitrogen content [38], which was not considered in this study and needs further investigation in the future. LAI retrieved from UAV multispectral imageries are indicative for biomass estimations, as presented in recent studies [13]. The simple linear equations generated from available measurements could be used to generate a spatial map of crop biomass. More ground measurements are, therefore, required to evaluate the accuracy of biomass maps, especially over plots not included in the correlation. Furthermore, the building of the relationship between biomass and yield is actually the interested target for real crop management and production.

5. Conclusions

This study proposed a method to generate a field map of LAI and CCC through PROSAIL radiative transfer model inversion based on an LUT method using UAV multispectral imageries. Three different distribution laws of LAI were evaluated as inputs to PROSAIL to generate the training database. The results showed that the dense uniform distribution provides the best estimations of LAI, validated by ground measurements, compared to uniform distribution and Gaussian distribution. The impacts of illumination conditions (e.g., clear or cloudy) on LAI and CCC estimations were then evaluated. The best retrieval strategy was found when using the clear sky PROSAIL model (diffuse ratio = 0) for UAV flights under clear sky conditions, and using the cloudy sky model (diffuse ratio = 1) for flights under cloudy sky conditions. The impacts of using the clear sky model for flights under cloudy illuminations were more obvious for large LAI (LAI > 5). We also demonstrated that CCC could be a good indicator for canopy nitrogen content estimations, and that LAI is meaningful for ground biomass mapping over the whole field.

Author Contributions: Conceptualization, W.L., M.W. and F.B.; methodology, W.L. and M.W.; software, W.L. and M.W.; formal analysis, W.L.; data curation, B.G. and L.C.; writing—original draft preparation, W.L.; writing—review and editing, M.W., B.G., L.C., J.J., W.W. and F.B.; project administration, F.B.; funding acquisition, F.B. All authors have read and agreed to the published version of the manuscript.

Funding: This work was funded by BPI France, Fonds Unitaire d'Investissement (FUI 17), under the project PRECIDRONE.

Data Availability Statement: Data sharing is not applicable to this article.

Acknowledgments: Wenjuan Li was supported by the National Natural Science Foundation of China (42201388) and Central Public-interest Scientific Institution Basal Research Fund (No. CAAS-ZDRW202107). We would like to thank Matthias Meulien, Aurore Argentin and Julio Valles for their valuable help during this study. We also thank Ovalie, Fred Venault and Kamran Irfan for ground measurements and DELAIR for drone acquisitions.

Conflicts of Interest: The authors declare no conflict of interest.

References

1. Mcbratney, A.; Whelan, B.; Ancev, T.; Mcbratney, A.; Bouma, J. Future Directions of Precision Agriculturew. *Precis. Agric.* **2005**, *6*, 7–23. [[CrossRef](#)]
2. Weiss, M.; Jacob, F.; Duveiller, G. Remote sensing for agricultural applications: A meta-review. *Remote Sens. Environ.* **2020**, *236*, 111402. [[CrossRef](#)]
3. Salamí, E.; Barrado, C.; Pastor, E. UAV Flight Experiments Applied to the Remote Sensing of Vegetated Areas. *Remote Sens.* **2014**, *6*, 11051–11081. [[CrossRef](#)]
4. Li, W.; Weiss, M.; Waldner, F.; Defourny, P.; Demarez, V.; Morin, D.; Hagolle, O.; Baret, F. A Generic Algorithm to Estimate LAI, FAPAR and FCOVER Variables from SPOT4_HRVIR and Landsat Sensors: Evaluation of the Consistency and Comparison with Ground Measurements. *Remote Sens.* **2015**, *7*, 15494–15516. [[CrossRef](#)]
5. Delloye, C.; Weiss, M.; Defourny, P. Retrieval of the canopy chlorophyll content from Sentinel-2 spectral bands to estimate nitrogen uptake in intensive winter wheat cropping systems. *Remote Sens. Environ.* **2018**, *216*, 245–261. [[CrossRef](#)]
6. Sun, L.; Gao, F.; Xie, D.; Anderson, M.; Chen, R.; Yang, Y.; Yang, Y.; Chen, Z. Reconstructing daily 30 m NDVI over complex agricultural landscapes using a crop reference curve approach. *Remote Sens. Environ.* **2021**, *253*, 112156. [[CrossRef](#)]
7. Li, W.; Baret, F.; Weiss, M.; Buis, S.; Lacaze, R.; Demarez, V.; Dejoux, J.-F.; Battude, M.; Camacho, F. Combining hectometric and decametric satellite observations to provide near real time decametric FAPAR product. *Remote Sens. Environ.* **2017**, *200*, 250–262. [[CrossRef](#)]
8. Gao, F.; Zhang, X. Mapping Crop Phenology in Near Real-Time Using Satellite Remote Sensing: Challenges and Opportunities. *J. Remote Sens.* **2021**, *2021*, 8379391. [[CrossRef](#)]
9. Xie, C.; Yang, C. A review on plant high-throughput phenotyping traits using UAV-based sensors. *Comput. Electron. Agric.* **2020**, *178*, 105731. [[CrossRef](#)]
10. Li, W.; Comar, A.; Weiss, M.; Jay, S.; Colombeau, G.; Lopez-Lozano, R.; Madec, S.; Baret, F. A Double Swath Configuration for Improving Throughput and Accuracy of Trait Estimate from UAV Images. *Plant Phenomics* **2021**, *2021*, 9892647. [[CrossRef](#)]

11. Guillen-Climent, M.L.; Zarco-Tejada, P.J.; Jimenez-Berni, J.A.; North, P.; Villalobos, F. Mapping radiation interception in row-structured orchards using 3D simulation and high-resolution airborne imagery acquired from a UAV. *Precis. Agric.* **2012**, *13*, 473–500. [[CrossRef](#)]
12. Verger, A.; Vigneau, N.; Chéron, C.; Gilliot, J.-M.; Comar, A.; Baret, F. Green area index from an unmanned aerial system over wheat and rapeseed crops. *Remote Sens. Environ.* **2014**, *152*, 654–664. [[CrossRef](#)]
13. Wan, L.; Zhang, J.; Dong, X.; Du, X.; Zhu, J.; Sun, D.; Liu, Y.; He, Y.; Cen, H. Unmanned aerial vehicle-based field phenotyping of crop biomass using growth traits retrieved from PROSAIL model. *Comput. Electron. Agric.* **2021**, *187*, 106304. [[CrossRef](#)]
14. Zarco-Tejada, P.J.; González-Dugo, V.; Berni, J.A.J. Fluorescence, temperature and narrow-band indices acquired from a UAV platform for water stress detection using a micro-hyperspectral imager and a thermal camera. *Remote Sens. Environ.* **2012**, *117*, 322–337. [[CrossRef](#)]
15. Chen, J.M.; Black, T.A. Defining leaf area index for non-flat leaves. *Plant Cell Environ.* **1992**, *15*, 421–429. [[CrossRef](#)]
16. Shadchina, T.M.; Dmitrieva, V.V. Leaf chlorophyll content as a possible diagnostic mean for the evaluation of plant nitrogen uptake from the soil. *J. Plant Nutr.* **1995**, *18*, 1427–1437. [[CrossRef](#)]
17. Gitelson, A.A.; Viña, A.; Ciganda, V.; Rundquist, D.C.; Arkebauer, T.J. Remote estimation of canopy chlorophyll content in crops. *Geophys. Res. Lett.* **2005**, *32*, L08403. [[CrossRef](#)]
18. Gitelson, A.A.; Peng, Y.; Huemmrich, K.F. Relationship between fraction of radiation absorbed by photosynthesizing maize and soybean canopies and NDVI from remotely sensed data taken at close range and from MODIS 250m resolution data. *Remote Sens. Environ.* **2014**, *147*, 108–120. [[CrossRef](#)]
19. Houllès, V.; Guérif, M.; Mary, B. Elaboration of a nitrogen nutrition indicator for winter wheat based on leaf area index and chlorophyll content for making nitrogen recommendations. *Eur. J. Agron.* **2007**, *27*, 1–11. [[CrossRef](#)]
20. Arroyo-Mora, J.P.; Kalacska, M.; Løke, T.; Schläpfer, D.; Coops, N.C.; Lucanus, O.; Leblanc, G. Assessing the impact of illumination on UAV pushbroom hyperspectral imagery collected under various cloud cover conditions. *Remote Sens. Environ.* **2021**, *258*, 112396. [[CrossRef](#)]
21. Hakala, T.; Honkavaara, E.; Saari, H.; Mäkynen, J.; Kaivosoja, J.; Pesonen, L.; Pölönen, I. Spectral Imaging from Uavs Under Varying Illumination Conditions. *ISPRS Int. Arch. Photogramm. Remote Sens. Spat. Inf. Sci.* **2013**, *XL-1/W2*, 189–194. [[CrossRef](#)]
22. Wang, S.; Baum, A.; Zarco-Tejada, P.J.; Dam-Hansen, C.; Thorseth, A.; Bauer-Gottwein, P.; Bandini, F.; Garcia, M. Unmanned Aerial System multispectral mapping for low and variable solar irradiance conditions: Potential of tensor decomposition. *ISPRS J. Photogramm. Remote Sens.* **2019**, *155*, 58–71. [[CrossRef](#)]
23. Darvishzadeh, R.; Matkan, A.A.; Ahangar, A.D. Inversion of a Radiative Transfer Model for Estimation of Rice Canopy Chlorophyll Content Using a Lookup-Table Approach. *IEEE J. Sel. Top. Appl. Earth Obs. Remote Sens.* **2012**, *5*, 1222–1230. [[CrossRef](#)]
24. Verrelst, J.; Camps-Valls, G.; Muñoz-Marí, J.; Rivera, J.P.; Veroustraete, F.; Clevers, J.G.P.W.; Moreno, J. Optical remote sensing and the retrieval of terrestrial vegetation bio-geophysical properties—A review. *ISPRS J. Photogramm. Remote Sens.* **2015**, *108*, 273–290. [[CrossRef](#)]
25. Combal, B.; Baret, F.; Weiss, M.; Trubuil, A.; Macé, D.; Pragnère, A.; Myneni, R.; Knyazikhin, Y.; Wang, L. Retrieval of canopy biophysical variables from bidirectional reflectance: Using prior information to solve the ill-posed inverse problem. *Remote Sens. Environ.* **2002**, *84*, 1–15. [[CrossRef](#)]
26. Verger, A.; Baret, F.; Camacho, F. Optimal modalities for radiative transfer-neural network estimation of canopy biophysical characteristics: Evaluation over an agricultural area with CHRIS/PROBA observations. *Remote Sens. Environ.* **2011**, *115*, 415–426. [[CrossRef](#)]
27. Duan, S.-B.; Li, Z.-L.; Wu, H.; Tang, B.-H.; Ma, L.; Zhao, E.; Li, C. Inversion of the PROSAIL model to estimate leaf area index of maize, potato, and sunflower fields from unmanned aerial vehicle hyperspectral data. *Int. J. Appl. Earth Obs. Geoinf.* **2013**, *26*, 12–20. [[CrossRef](#)]
28. *Minolta SPAD 502 MANUAL*; Industrial Meter, Ramsey; Minolta Corp: Macquarie Park, Australia, 2009.
29. Cerovic, Z.G.; Masdoumier, G.; Ben Ghazlen, N.; Latouche, G. A new optical leaf-clip meter for simultaneous non-destructive assessment of leaf chlorophyll and epidermal flavonoids. *Physiol. Plant.* **2012**, *146*, 251–260. [[CrossRef](#)] [[PubMed](#)]
30. Schaepman-Strub, G.; Schaepman, M.E.; Painter, T.H.; Dangel, S.; Martonchik, J.V. Reflectance quantities in optical remote sensing—definitions and case studies. *Remote Sens. Environ.* **2006**, *103*, 27–42. [[CrossRef](#)]
31. Verhoef, W. Light scattering by leaf layers with application to canopy reflectance modeling: The SAIL model. *Remote Sens. Environ.* **1984**, *16*, 125–141. [[CrossRef](#)]
32. Jacquemoud, S.; Verhoef, W.; Baret, F.; Bacour, C.; Zarco-Tejada, P.J.; Asner, G.P.; François, C.; Ustin, S.L. PROSPECT + SAIL models: A review of use for vegetation characterization. *Remote Sens. Environ.* **2009**, *113* (Suppl. S1), S56–S66. [[CrossRef](#)]
33. Jacquemoud, S.; Baret, F. PROSPECT: A model of leaf optical properties spectra. *Remote Sens. Environ.* **1990**, *34*, 75–91. [[CrossRef](#)]
34. Weidong, L.; Baret, F.; Xingfa, G.; Qingxi, T.; Lanfen, Z.; Bing, Z. Relating soil surface moisture to reflectance. *Remote Sens. Environ.* **2002**, *81*, 238–246. [[CrossRef](#)]
35. Weiss, M.; Baret, F.; Myneni, R.; Pragnère, A.; Knyazikhin, Y. Investigation of a model inversion technique to estimate canopy biophysical variables from spectral and directional reflectance data. *Agron.* **2000**, *20*, 3–22. [[CrossRef](#)]
36. Sinha, S.K.; Padalia, H.; Dasgupta, A.; Verrelst, J.; Rivera, J.P. Estimation of leaf area index using PROSAIL based LUT inversion, MLRA-GPR and empirical models: Case study of tropical deciduous forest plantation, North India. *Int. J. Appl. Earth Obs. Geoinf.* **2019**, *86*, 102027. [[CrossRef](#)] [[PubMed](#)]

37. Wang, L.; Chen, S.; Li, D.; Wang, C.; Jiang, H.; Zheng, Q.; Peng, Z. Estimation of Paddy Rice Nitrogen Content and Accumulation Both at Leaf and Plant Levels from UAV Hyperspectral Imagery. *Remote Sens.* **2021**, *13*, 2956. [[CrossRef](#)]
38. Clevers, J.G.P.W.; Kooistra, L. Using Hyperspectral Remote Sensing Data for Retrieving Canopy Chlorophyll and Nitrogen Content. *IEEE J. Sel. Top. Appl. Earth Obs. Remote Sens.* **2012**, *5*, 574–583. [[CrossRef](#)]

Disclaimer/Publisher’s Note: The statements, opinions and data contained in all publications are solely those of the individual author(s) and contributor(s) and not of MDPI and/or the editor(s). MDPI and/or the editor(s) disclaim responsibility for any injury to people or property resulting from any ideas, methods, instructions or products referred to in the content.